Intermolecular Interactions Involved in Solute Retention on Carbon Media in Reversed-Phase High-Performance Liquid Chromatography

ARTICLE *in* ANALYTICAL CHEMISTRY · MARCH 1997

Impact Factor: 5.64 · DOI: 10.1021/ac960453f · Source: PubMed

4 AUTHORS, INCLUDING:

Paul Timothy Jackson
St. Olaf College
14 PUBLICATIONS **267** CITATIONS
SEE PROFILE

Peter W Carr
University of Minnesota Twin Cities
424 PUBLICATIONS **13,517** CITATIONS
SEE PROFILE

Anal. Chem. **1997,** *69,* 416−425

Intermolecular Interactions Involved in Solute Retention on Carbon Media in Reversed-Phase High-Performance Liquid Chromatography

Paul T. Jackson, Mark R. Schure,[†] Thomas P. Weber,[‡] and Peter W. Carr*

Department of Chemistry, University of Minnesota, 207 Pleasant Street SE, Minneapolis, Minnesota 55455

Carbon adsorbents for RPLC separations are greatly underutilized due to the poor chromatographic properties of the earliest commercially available materials and our limited understanding of solute interactions with the solid surface. Previously, we reported on the properties of a carbon surface prepared by vapor deposition on porous zirconia microspheres. The resulting material is a new type of carbon sorbent with considerably improved chromatographic properties. Here we present a fundamental study of the intermolecular interactions influencing solute retention on these novel carbon phases under RPLC conditions. Retention on seven unique carbon phases has been correlated with solute descriptors of dispersion, dipolarity/polarizability, and hydrogen bond basicity through the use of linear solvation energy relationships (LSERs). In stark contrast, conventional bonded phases do not show the large contribution from dipolarity/polarizability that is observed on these types of carbon. The presence of this interaction indicates a distinct difference between carbon and conventional bonded RPLC phases. Other results suggest that solvent sorption plays a significant role in controlling solute retention on carbon. In addition, we investigated the temperature dependence of retention on carbon and found typical RPLC-like behavior.

A variety of important processes utilize carbon-based sorbents. For example, the pulp, paper, and petroleum industries as well as chemical manufacturers remove environmentally hazardous chemicals from wastewaters with such sorbents.[1] Drinking water suppliers employ carbon filters to capture undesirable chemicals. Environmental analysts use graphitic carbon solid phase extraction cartridges for sample preconcentration and cleanup.[2−4] Carbon-based stationary phases show unique selectivity for solutes in gas, liquid, and supercritical fluid chromatographic analyses.[5−7] It is the nature of the solute interactions with this truly remarkable and versatile sorbent that lies at the heart of its use.

The well-known limitations of silica gel in liquid chromatography have motivated our study of carbon sorbents. Many research groups have attempted to prepare carbon sorbents suitable for high-performance liquid chromatography (HPLC); however, the demands placed on the material by the analytical technique have thus far led to the development of only one commercially available phase.[8−13] Carbon phases do not exhibit the pH instability problems of silica gel and some other metal oxide particles; they do not dissolve at high pH and do not hydrolyze under strongly acidic conditions. This extends the operational pH range of liquid chromatographic analyses and circumvents the use of synthetic polymeric supports that can shrink and swell as the solvent, pH, and ionic strength are changed. Most significantly and most poorly appreciated is the unprecedented the ability of carbon sorbents to separate structurally similar species. The durability of this sorbent coupled to its selectivity ought to make it extremely attractive to the chemical community and, in particular, to chromatographers.

Over the last several years, our laboratory has been engaged in developing zirconia-based carbon HPLC sorbents.[14−20] Many factors have contributed to our interest in these materials. First, the carbon deposit "seals" the metal oxide surface from solutes and virtually eliminates the problematic hard Lewis acid−base interactions.[17,21−23] Second, the manufacturing process, chemical vapor deposition (CVD), is much simpler and more cost effective than the template polymerization method of Knox et al.[13] Ad-

[†] Present address: Theoretical Separation Science Laboratory, Rohm & Haas Company, 727 Norristown Rd., Spring House, PA 19477.

[‡] Present address: CIMA Laboratories, 7325 Aspen L., Brooklyn Park, MN 55428.

(1) Austin, G. T. *Chreve's Chemical Process Industries*, 5th ed.; McGraw-Hill: New York, 1984; Chapter 3.
(2) DiCorcia, A.; Samperi, R.; Marcomini, A.; Stelluto, S. *Anal. Chem.* **1993**, *65*, 907−912.
(3) Hennion, M. C.; Guenu, S. *J. Chromatogr. A* **1994**, *665*, 243−251.
(4) DiCorcia, A.; Samperi, R.; Marchese, S. *J. Chromatogr. A* **1993**, *642*, 163−174.
(5) Kiselev, A. V.; Yashin, Y. I. *Gas-Adsorption Chromatography*; Plenum: New York, 1969.
(6) Tanaka, N.; Tanigawa, T.; Kimata, K.; Hosoya, K.; Araki, T. *J. Chromatogr.* **1991**, *549*, 29−41.
(7) Olesik, S. V.; Engel, T. M.; Callstrom, M. R.; Diener, M. *Anal. Chem.* **1993**, *65*, 3691−3700.
(8) Colin, H.; Ward, N.; Guiochon, G. *J. Chromatogr.* **1978**, *149*, 169−197.
(9) Colin, H.; Eon, C.; Guiochon, G. *J. Chromatogr.* **1976**, *119*, 41−54.
(10) Unger, K. K.; Roumeliotis, P.; Mueller, H.; Goetz, H. *J. Chromatogr.* **1980**, *202*, 3−14.
(11) Leboda, R. *Mater. Chem. Phys.* **1992**, *31*, 243−255.
(12) Leboda, R. *Mater. Chem. Phys.* **1993**, *34*, 123−141.
(13) Knox, J. H.; Kaur, B.; Millward, G. R. *J. Chromatogr.* **1986**, *352*, 3−25.
(14) Weber, T. P.; Carr, P. W.; Funkenbusch, E. F. *J. Chromatogr.* **1990**, *519*, 31−52.
(15) Weber, T. P.; Carr, P. W. *Anal. Chem.* **1990**, *62*, 2620−2625.
(16) Weber, T. P. Ph.D. Thesis, University of Minnesota, Minneapolis, MN, 1991.
(17) Weber, T. P.; Jackson, P. T.; Carr, P. W. *Anal. Chem.* **1995**, *67*, 3042−3050.
(18) Funkenbusch, E. F.; Carr, P. W.; Hanggi, D.; Weber, T. P. U.S. Patent 5 108 597, 1992.
(19) Funkenbusch, E. F.; Carr, P. W.; Hanggi, D.; Weber, T. P. U.S. Patent 5 182 016, 1993.
(20) Funkenbusch, E. F.; Carr, P. W.; Hanggi, D.; Weber, T. P. U.S. Patent 5 254 262, 1993.
(21) Nawrocki, J.; Rigney, M. P.; McCormick, A.; Carr, P. W. *J. Chromatogr. A* **1993**, *657*, 229−282.
(22) Blackwell, J. A.; Carr, P. W. *J. Chromatogr.* **1992**, *596*, 27−41.
(23) Blackwell, J. A.; Carr, P. W. *Anal. Chem.* **1992**, *64*, 853−862.

S0003-2700(96)00453-2 CCC: $14.00

ditionally, we hoped that the coated zirconia might have efficiencies and selectivities similar to those of porous graphitic carbon (PGC). Finally, the particle and pore structures of the material are pre-established by the underlying metal oxide, thereby eliminating dependencies on the carburization or graphitization process.

In addition to its use as a stationary phase in liquid chromatography, it is important to understand how chemicals interact with carbon because it is a ubiquitous sorbent. These interactions drive process design and dictate the sorbent's effectiveness for specific tasks. By investigating surface−molecule interactions, we can learn how to better utilize this material and begin to predict how changes in the system will influence carbon-based separation processes.

This work compares the retention of solutes on PGC and ODS silica to those on various carbon-clad zirconia chromatographic phases (denoted C/ZrO_2) obtained by CVD of carbon on porous ZrO_2 particles. A variety of C/ZrO_2 phases, made using the same base porous ZrO_2 particles but differing only in the source of carbon for the CVD reaction, were studied here. The chromatographic nature of the carbon-coated materials is examined through solvatochromic analysis and temperature studies in an attempt to explain the unique chromatographic character of these and other carbon phases.

EXPERIMENTAL SECTION

Reagents. The chemicals used in this study were obtained from the following suppliers: acetonitrile (ACN) and tetrahydrofuran (THF) were HPLC grade and obtained from Fisher Scientific (Fairlawn, NJ); methanol (Chromar grade) was obtained from Mallinckrodt (Paris, KY). The unstabilized THF was tested for peroxides before use. Water for the HPLC mobile phase was purified by passing house-deionized water through a Barnstead/Thermolyne Nanopure (Dubuque, IA) water purification system with an "organic-free" final cartridge, followed by a 0.2 μm particle filter. All solutes for the chromatographic studies were obtained from Aldrich Chemical Co. (Milwaukee, WI) and used without further purification. Sample concentrations were minimal (<10 mM), and samples were diluted in the mobile phase used.

Chromatographic Support Preparation. The CVD process utilizes a tube furnace in which volatile organic compounds are passed over porous ZrO_2 particles at an elevated temperature (~700 °C) and at reduced pressure (~5−10 Torr). This procedure creates a uniform carbon coating on the porous particles in which it is possible to achieve >97% coverage of the available ZrO_2 surface while still retaining the pore structure of the particles.[17] Vapor sources used for deposition include heptane (Hp), isooctane (Io), cyclopentane (Cp), 1-butanol (B), toluene (T), and 1,7-octadiene (Od). After completion of the deposition process, the carbon-coated particles were Soxhlet extracted with either tetrahydrofuran or heptane. The material was packed into a column and used as a reversed-phase support.

For purposes of comparison, two commercially available chromatographic materials were examined. Porous graphitic carbon (Hypercarb) was obtained from Keystone Scientific Inc. (Bellefonte, PA). It is made by the silica gel template method of Knox et al.[13] The other phase, ODS-Hypersil (Shandon Scientific Ltd., Runcorn, Cheshire, U.K.) is a silica-based, chemically bonded octadecyl reversed-phase material. A variety of C/ZrO_2 phases made from the same base porous ZrO_2 particles were studied; their identity and physical characteristics have been previously reported.[17]

Chromatographic Studies. All studies were conducted on a Hewlett-Packard (Palo Alto, CA) 1090 high-performance liquid chromatograph with a DR5 solvent delivery system and a filter photometric detector. The chromatographic parameters were averages of at least triplicate determinations of each solute, and detection was at 254 or 210 nm. Absorbance data from the filter photometric detector were digitized, integrated, and plotted with a Hewlett-Packard 3393A integrator that controlled the liquid chromatograph through an HP-IL interface loop. Digitized data were stored on a Hewlett-Packard 9153A disk drive connected to the HP-IL interface loop. Column dead time was measured from both solvent mismatch and deuterium oxide peaks.

RESULTS AND DISCUSSION

Solvatochromic Analysis. Solvatochromic linear solvation energy relationships (LSERs)[24] were used to determine the contributions of various molecular descriptors to retention on the RPLC phases. Based on previous studies,[25−27] the LSER equation is expected to take the following form:

$$\log k' = \log k_0' + mV_x + s\pi_2^* + a\sum\alpha_2^H + b\sum\beta_2^H \quad (1)$$

where V_x is the solute molecular volume calculated using McGowan's algorithm,[28] π_2^* is the solute dipolarity/polarizability descriptor, $\sum\alpha_2^H$ is the solute's ability to donate a hydrogen bond, and $\sum\beta_2^H$ is a measure of solute hydrogen bond-accepting strength. Values for V_x, π_2^*, $\sum\alpha_2^H$, and $\sum\alpha_2^H$ were taken from Abraham et al. and are listed in Table 1.[29] The fitting coefficients, **log** k_0', m, s, a, and b, reflect the difference in a specific bulk property between the stationary and mobile phases; the specific bulk property is that which is the solute's complement (i.e., solute hydrogen bond acidity's complement is mobile and stationary phase hydrogen bond basicity). Tables 1 and 2 give the solute descriptors and the variance−covariance matrix, respectively.

Retention on conventional bonded-phase RPLC media was analyzed previously through use of eq 1.[25−27] For ODS-Hypersil data, residual analysis indicates that *N*-methylaniline is an outlier and must be eliminated. This is not surprising given the high level of silanophilicity generally exhibited by Hypersil bonded phases.[30] After removing this single outlier, regression analysis yields the results reported in Table 3, and they agree well with previously reported analyses.[25] Note the excellent goodness-of-fit parameters, specifically the correlation coefficient and average standard deviation (r > 0.99, $\overline{sd}$ < 0.06).

The applicability of the basic LSER equation to correlating retention on carbon is questionable since the proposed mechanism of retention is adsorption. This particular LSER expression (eq 1) utilizes solute descriptors measured in systems where the solutes are retained by primarily partitioning phenomena (GLC,

(24) Carr, P. W. *Microchem. J.* **1993**, *48*, 4−28.
(25) Tan, L. C. Ph.D. Thesis, University of Minnesota, Minneapolis, MN, 1994.
(26) Sadek, P. C.; Carr, P. W.; Doherty, R. M.; Kamlet, M. J.; Taft, R. W.; Abraham, M. H. *Anal. Chem.* **1985**, *57*, 2971−2978.
(27) Carr, P. W.; Doherty, R. M.; Kamlet, M. J.; Taft, R. W.; Melander, W.; Horvath, C. *Anal. Chem.* **1986**, *58*, 2674−2680.
(28) McGowan, J. C.; Abraham, M. H. *Chromatographia* **1987**, *23*, 243−246.
(29) Abraham, M. H.; Andonian-Haftvan, J.; Whiting, G. S.; Leo, A; Taft, R. W. *J. Chem. Soc., Perkin Trans. 2* **1994**, 1777−1791.
(30) Snyder, L. R.; Stadalius, M. A.; Berus, J. S. *LC-GC* **1988**, *6*, 494−500.

Table 1. Chromatographic Solutes and LSER Descriptors

no.	solute	V_x[a]	π_2^*[b]	$\sum\alpha_2^H$[c]	$\sum\beta_2^H$[d]	R_2[e]	SA1[f]	SA2[g]
1	benzene	0.716	0.52	0.00	0.14	0.844	0.511	0.368
2	toluene	0.857	0.52	0.00	0.14	0.843	0.573	0.422
3	ethylbenzene	0.998	0.51	0.00	0.15	0.843	0.636	0.477
4	propylbenzene	1.139	0.50	0.00	0.15	0.843	0.708	0.542
5	butylbenzene	1.280	0.51	0.00	0.15	0.843	0.774	0.602
6	pentylbenzene	1.421	0.51	0.00	0.15	0.843	0.843	0.665
7	acetophenone	1.014	1.01	0.00	0.49	0.741	0.664	0.501
8	propiophenone	1.155	0.95	0.00	0.51	0.741	0.730	0.560
9	butyrophenone	1.296	0.95	0.00	0.51	0.741	0.798	0.622
10	valerophenone	1.437	0.95	0.00	0.51	0.741	0.867	0.686
11	hexanophenone	1.577	0.95	0.00	0.51	0.741	0.936	0.750
12	fluorobenzene	0.734	0.57	0.00	0.10	0.529	0.537	0.389
13	chlorobenzene	0.839	0.65	0.00	0.07	0.910	0.571	0.420
14	bromobenzene	0.891	0.73	0.00	0.09	0.994	0.587	0.434
15	iodobenzene	0.975	0.82	0.00	0.12	1.597	0.609	0.454
16	phenol	0.775	0.89	0.60	0.31	0.772	0.547	0.399
17	benzyl alcohol	0.916	0.87	0.33	0.56	0.772	0.610	0.454
18	3-phenylpropanol	1.198	0.90	0.30	0.67	0.772	0.750	0.579
19	styrene	0.955	0.65	0.00	0.16	1.013	0.651	0.489
20	biphenyl	1.324	0.99	0.00	0.22	1.687	0.852	0.667
21	benzonitrile	0.871	1.11	0.00	0.33	0.730	0.594	0.441
22	nitrobenzene	0.891	1.11	0.00	0.28	0.563	0.621	0.463
23	anisole	0.916	0.75	0.00	0.29	0.772	0.610	0.454
24	4-nitrotoluene	1.031	1.11	0.00	0.28	0.556	0.685	0.519
25	4-nitrophenol	0.949	1.72	0.82	0.26	0.549	0.657	0.495
26	*N*-methylaniline	0.957	0.90	0.17	0.43	0.735	0.637	0.477

[a] Molecular volume. [b] Dipolarity/polarizability. [c] Hydrogen bond acidity. [d] Hydrogen bond basicity. [e] Excess polarizability calculated from eq 2. [f] Projected surface area calculated using $r_p = 0.61$. [g] Projected surface area calculated using $r_p^{\ddagger} = 0.61$.

Table 2. Variance–Covariance Matrix of LSER Solute Descriptors[a]

	V_x	π_2^*	$\sum\alpha_2^H$	$\sum\beta_2^H$	SA1	SA2	R_2
V_x	1.000	0.066	−0.208	0.401	0.991	0.992	0.150
π_2^*		1.000	0.563	0.465	0.149	0.142	−0.207
$\sum\alpha_2^H$			1.000	0.232	−0.167	−0.169	−0.238
$\sum\beta_2^H$				1.000	0.424	0.422	−0.305
SA1					1.000	1.000	0.132
SA2						1.000	0.128
R_2							1.000

[a] Note there is high covariance between V_x, SA1, and SA2.

conventional RPLC, octanol–water partition coefficients); however, it is extremely unlikely that solutes partition into the rigid nonporous sheath carbon. Furthermore, there may well be orientational effects in the solute sorption on the surface similar to Snyder's proposal that solutes localize in LSC on silica and alumina.[31] Thus, the use of a volume parameter to model cavity formation and dispersion forces as well as the use of the π_2^* parameter to model dipolarity/polarizability may be incomplete and lead to poor fits. Since hydrogen bonding interactions are highly orientational in nature, they are probably well modeled by the traditional partition-derived parameters. In an attempt to compensate for the potential limitations of the LSER model, we examined additional solute descriptors.

Literature on carbon sorbents suggests significant electronic or charge transfer-type interactions.[6,32,33] Based on that information, solute excess polarizabilities, R_2, were computed from average molecular polarizabilities calculated from Miller and Savchik.[34] R_2 indicates the polarizability above that represented by a linear alkane of the same molecular volume (eq 2) and should

$$R_2 = \rho_{\text{solute},V_x} - \rho_{\text{alkane},V_x} \qquad (2)$$

account for additional electronic interactions between the solutes and the carbon surface. This quantity correlates well with those reported by Abraham et al.;[29] we use this excess value since ref 29 did not contain values for all solutes of interest.

Carbon sorbents, especially graphitic adsorbents, are considered locally flat, and we suspect that the use of the solute molecular volume descriptor does not model dispersive interactions at all well. The projected surface area, also referred to as the cross-sectional surface area, has been discussed many times in the context of surface chemistry[35] and chromatography;[31] the values are tabulated (see Table 1) for the solutes used herein. The methodology needed to compute this quantity has been discussed previously in the literature and consists of methods which include molecular modeling[36] and fractal mathematics.[37] Our approach here is similar to that of ref 36, where molecular modeling was used to produce a van der Waals cross section, and then the models were printed, and the weight of the paper was denoted to be proportional to the integrated cross-sectional area. A calibration constant was then used to bring the experimental cross-sectional area into agreement with the weight of the paper. In our approach, the entire procedure is via calculation as we use a separate computer program that reads the molecular modeling structures from a disk. A complete description of the procedure for calculating cross-sectional surface area is given in the Appendix.

No combination of solute descriptors for correlating retention on carbon phases gave fits as good as those obtained for bonded RPLC phases.[25] High correlation between solute volume and projected surface areas prevented the use of both parameters in a single LSER. Residual analysis by least-squares and least-median algorithms provided little insight into improving the fits; therefore, we decided to use only the more traditional solute descriptors, that is, those used previously in the study of bonded phases. Use of eq 1 allows comparison to other systems including ODS phases. Multiple linear regression of log k' for 26 solutes against the LSER solute descriptors from Table 1 indicated that all parameters were significant, and the fits were consistent with LSERs performed on other carbon materials.[7,38,39]

The fitting coefficients, standard error of the fit, and correlation coefficients for all packings can be found in Table 3. The data indicate that a combination of three solute descriptors, size (molecular volume), dipolarity/polarizability, and hydrogen bond basicity, dictate a solute's retention. However, the large average error of the fits and the poor standard deviations of the coefficients

(31) Snyder, L. R. *Principles of Adsorption Chromatography*; Marcel Dekker: New York, 1968.
(32) Hennion, M. C.; Coquart, V.; Guenu, S.; Sella, C. *J. Chromatogr. A* **1995**, *712*, 287–301.
(33) Kaliszan, R.; Osmailowski, K.; Bassler, B. J.; Hartwick, R. A. *J. Chromatogr.* **1990**, *499*, 333–344.
(34) Miller, K. J.; Savchik, J. A. *J. Am. Chem. Soc.* **1979**, 7206–7213.
(35) McClellan, A. L.; Harnsberger, H. F. *J. Colloid Interface Sci.* **1976**, *23*, 577.
(36) Gray, M. J.; Mebane, R. C.; Womack, H. N.; Rybolt, T. R. *J. Colloid Interface Sci.* **1995**, *170*, 98–101.
(37) Meyer, A. M.; Farin, D.; Avnir, D. *J. Am. Chem. Soc.* **1986**, *108*, 7897–7905.
(38) Luehrs, D. C.; Hickey, J. P.; Nilsen, P. E.; Godbole, K. A.; Rogers, T. N. *Environ. Sci. Technol.* **1996**, *30*, 143–152.
(39) Kamlet, M. J.; Taft, R. W.; Abraham, M. H. *Carbon* **1985**, *23*, 549–554.

Table 3. LSER Regression Results for All Columns[a]

phase	log k_0'	m	s	a	b	n[b]	sd[c]	r[d]
			65% ACN					
Hp-C/ZrO_2	−2.02 (0.14)	1.79 (0.13)	1.17 (0.12)	−0.66 (0.16)	−1.39 (0.18)	26	0.13	0.968
Io-C/ZrO_2	−2.07 (0.13)	1.76 (0.11)	1.15 (0.11)	−0.61 (0.14)	−1.39 (0.16)	26	0.11	0.973
B-C/ZrO_2	−2.04 (0.13)	1.79 (0.11)	1.17 (0.11)	−0.66 (0.14)	−1.40 (0.16)	26	0.11	0.975
Cp-C/ZrO_2	−2.04 (0.12)	1.70 (0.11)	1.09 (0.10)	−0.63 (0.13)	−1.32 (0.15)	26	0.11	0.974
T-C/ZrO_2	−2.10 (0.12)	1.82 (0.11)	1.19 (0.10)	−0.72 (0.13)	−1.66 (0.15)	26	0.11	0.977
Od-C/ZrO_2	−2.30 (0.11)	1.79 (0.10)	1.20 (0.10)	−0.84 (0.12)	−1.61 (0.14)	26	0.10	0.981
Hypercarb	−2.24 (0.24)	2.03 (0.21)	0.97 (0.20)	−0.57 (0.26)	−1.40 (0.30)	26	0.21	0.928
ODS-Hypersil	−0.72 (0.04)	1.35 (0.04)	−0.28 (0.04)	−0.55 (0.05)	−1.50 (0.05)	25	0.04	0.997
			36% THF					
Hp-C/ZrO_2	−1.17 (0.16)	1.89 (0.15)	0.63 (0.14)	−0.45 (0.18)	−1.88 (0.20)	26	0.14	0.957
Io-C/ZrO_2	−1.23 (0.12)	1.86 (0.11)	0.64 (0.11)	−0.35 (0.13)	−1.92 (0.16)	26	0.11	0.973
B-C/ZrO_2	−1.17 (0.15)	1.86 (0.13)	0.62 (0.11)	−0.39 (0.16)	−1.84 (0.19)	26	0.13	0.963
Cp-C/ZrO_2	−1.18 (0.14)	1.72 (0.13)	0.61 (0.12)	−0.38 (0.16)	−1.73 (0.18)	26	0.13	0.959
T-C/ZrO_2	−1.20 (0.19)	1.75 (0.17)	0.86 (0.16)	−0.63 (0.21)	−2.06 (0.24)	26	0.17	0.941
Od-C/ZrO_2	−2.30 (0.16)	1.70 (0.14)	0.73 (0.13)	−0.56 (0.17)	−1.96 (0.20)	26	0.14	0.956
Hypercarb	−1.38 (0.15)	2.01 (0.14)	0.59 (0.13)	−0.51 (0.17)	−1.92 (0.19)	26	0.13	0.966
ODS-Hypersil	−0.16 (0.06)	1.39 (0.05)	−0.24 (0.05)	−0.04 (0.06)	−1.77 (0.08)	25	0.05	0.992
			83% MeOH					
Hp-C/ZrO_2	−2.12 (0.17)	1.93 (0.15)	1.19 (0.14)	−0.51 (0.18)	−1.23 (0.20)	26	0.15	0.962
Io-C/ZrO_2	−2.17 (0.16)	1.83 (0.14)	1.18 (0.13)	−0.49 (0.17)	−1.19 (0.20)	26	0.14	0.964
B-C/ZrO_2	−2.17 (0.15)	1.87 (0.14)	1.19 (0.13)	−0.53 (0.17)	−1.16 (0.19)	26	0.14	0.966
Cp-C/ZrO_2	−2.17 (0.15)	1.79 (0.14)	1.17 (0.13)	−0.53 (0.17)	−1.16 (0.19)	26	0.14	0.965
T-C/ZrO_2	−1.91 (0.24)	1.67 (0.22)	1.33 (0.21)	−1.01 (0.27)	−1.32 (0.31)	26	0.22	0.920
Od-C/ZrO_2	−2.87 (0.23)	2.01 (0.21)	1.87 (0.20)	−0.72 (0.26)	−1.88 (0.30)	26	0.21	0.949
Hypercarb	−2.71 (0.24)	2.23 (0.21)	1.39 (0.20)	−0.62 (0.26)	−1.42 (0.30)	26	0.21	0.944

[a] Coefficients with single standard deviation in parentheses. [b] Number of solutes. [c] Average standard deviation of the fit. [d] Correlation coefficient of the fit.

preclude the use of the LSER approach to distinguish between the different types of carbon phases (saturated, unsaturated, porous graphitic), as reported in previous work.[16,17] Figure 1 compares the predicted LSER solute retention to the experimental values obtained for ODS-Hypersil and carbon phases; these results are typical of all the data analyzed in this work. Virtually all solutes, regardless of functional group, fall on or in close proximity to the one-to-one line for ODS-Hypersil. In contrast, Figure 1B shows considerable scatter around the one-to-one line and represents the lack of fit when using eq 1 to correlate data for a carbon phase. As evident from both parts of Figure 1, no specific solute class or classes contribute significantly to the variance.

As stated earlier, there are two plausible explanations for the lack of fit exhibited by the carbon data. Our experimental retention factors might be imprecise, or the model itself might be wrong and/or the solute descriptive parameters incorrect. If random errors in the measurement of the retention factors were the major problem, then correlations of log k' on one phase versus those on a second must also be poor. The representative linear regression plots, shown in Figure 2, indicate that solute retentions on the various carbon phases are very highly correlated. When the sole deviant point (nitrotoluene) is excluded, extremely good correlations are obtained, as shown in Table 4. Thus, we conclude that the relatively poor LSER correlations on carbon are not due to experimental imprecision. Furthermore, we believe that the results above are the best that can be achieved with eq 1 and current solute parameters. The LSER analysis of the ODS-Hypersil retention factors suggests that we have good quality data and that the problem with the analysis of carbon packings resides in the model.

The slopes, correlation coefficients, and standard deviations given in Table 4 indicate that all the carbon phases display, in Horvath's terminology, "homeoenergetic" behavior.[40] Characteristics of this behavior are good linear correlations with a slope different from unity. This implies that the physicochemical basis for solute retention is similar on all the carbon phases. Poor correlations are observed between any carbon phase and the ODS-Hypersil. Thus, the physicochemical basis of solute retention is different on these materials.

Even though our LSER approach does not fit the data well, we can make some generalizations about the physicochemical processes influencing solute retention. We first examine the LSER coefficients for all materials at a single mobile phase compositions and then look at different mobile phases. Figure 3 shows a cross-column comparison of the LSER regression coefficients; standard deviations are not shown for readability. Data for ODS-Hypersil in 83:17 (v/v) methanol/water were not used due to low retention and the high uncertainties associated with small retention factors.

McGowan Volume (mV_x). This parameter represents two processes: cavity formation and dispersion interactions. It is of considerable magnitude and positive for all phases examined; therefore, an increase in solute size leads to an increase in retention. The magnitude of the coefficient is smaller for the ODS phase than for the carbon phases; this must originate in the stationary phase, since the packings are compared in the same mobile phases. Because the m coefficient on the carbon phases is so much larger than that on the conventional phase, we conclude that carbon phases are effectively much more "hydrophobic" than alkyl bonded phases. Since we do not know the exact manner in which the solutes adsorb on the carbon surface, the difference between m on the bonded phase and the carbon phases could arise from any of three possible phenomena. The m coefficient might be larger because the energy needed to merely

(40) Horvath, Cs.; Melander, W. R.; Stoveken, J. *J. Chromatogr.* **1980**, *199*, 35−56.

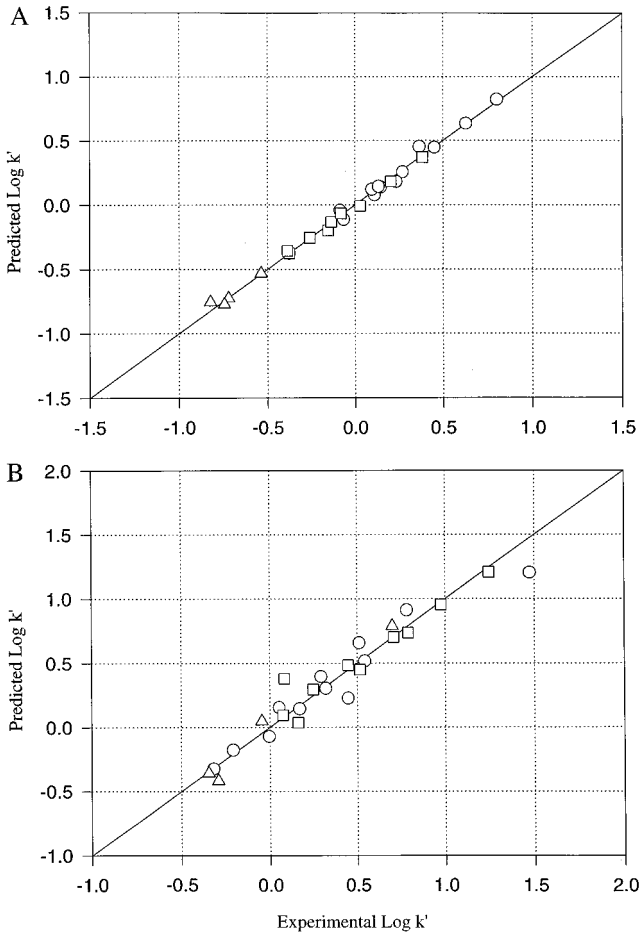

Figure 1. Plot of log K_{pred} based on the LSER versus log K_{exp}. Conditions: 65:35 ACN/water mobile phase, 1 mL min^{-1}, 30 °C, 5 μL injections, 254 nm detection. Symbols: ○, nonpolar solutes; △, hydrogen bond donors; and □, polar solutes. Curve A, ODS-Hypersil. Curve B, Hp-C/ZrO_2.

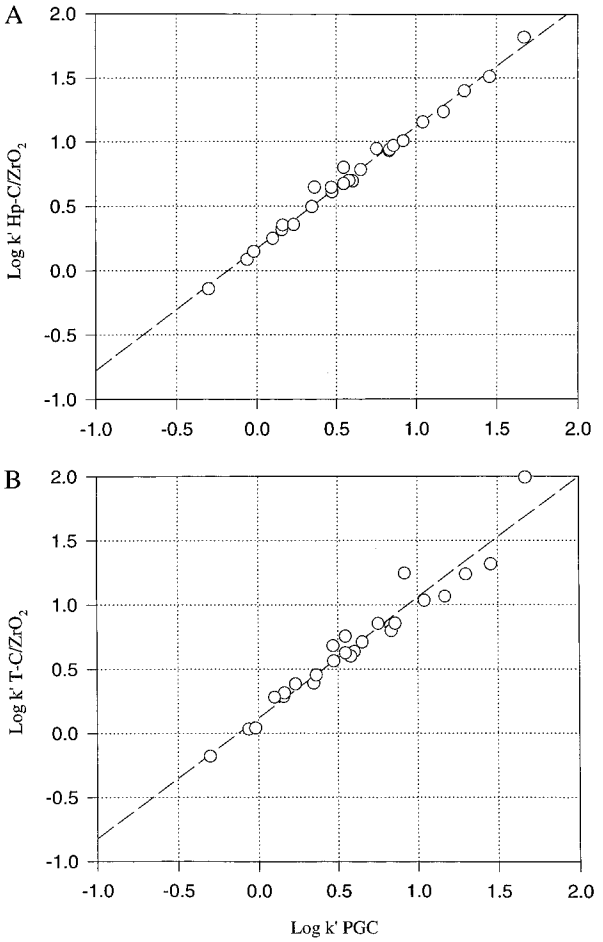

Figure 2. Plot of log K' on C/ZrO_2 versus log K' on Hypercarb. Conditions: 36:64 THF/water, all else same as in Figure 1. Curve A, Hp-C/ZrO_2. Curve B, T-C/ZrO_2.

displace sorbed eluent from the surface in an adsorption process would be smaller than the energy needed to make a cavity in a partition process. Second, the dispersion forces involved in solute adsorption on carbon may be larger than those associated with sorption into an alkane-like bonded phase. Third, a combination of the previous two factors, eluent displacement and added dispersive strength, would also yield the same result. The *m* coefficient is almost the same in the different mobile phases; this is not surprising since the mobile phase compositions were selected in order to make the methylene unit selectivity the same. Since the *m* coefficient tracks the hydrophobic selectivity and that selectivity is represented by the methylene increment, we expect the results to show that the *m* coefficient varies with methylene selectivity.

Dipolarity/Polarizability ($s\pi_2^*$). The large magnitude and the positive sign of this term for all carbon adsorbents stands in stark contrast to the small size and negative sign invariably observed for this term with all alkyl bonded phase RPLC packings.[26−28] On carbon phases, an increase in solute dipolarity/polarizability (π_2^*) causes a *considerable increase* in retention. A similar increase in solute π_2^* causes a *small decrease* in retention on conventional bonded phases. The large, positive *s* coefficient indicates a significant electronic component to retention. This coefficient is very sensitive to the mobile phase. The *s* coefficients of all carbon phases are virtually identical in both MeOH and ACN mobile phases but decrease by about a factor of 2 in the THF mobile phase. This phenomenon is very likely linked to the ability of the modifier to wet the carbon surface.[17] Furthermore, Knox and Kaur[41] and Guiochon et al.[42] assert that THF is a very strong eluent on carbon phases. Wetting of the carbon surface can potentially result in two effects: (1) the THF molecules will act as better displacing agents for solutes strongly sorbed to the carbon surface due to electronic interactions, and (2) the carbon surface may have a fixed layer of sorbed THF that attenuates the strong sorptive nature of the carbon. Both effects would serve to decrease solute retention.

Hydrogen Bond Basicity ($b\sum_2^H$). This coefficient is large and negative in all cases. It is controlled by the complementary system property, in this case the hydrogen bond acidity of the aqueous/organic mobile phase, and will be influenced by the mobile phase composition.[43] Since water is the strongest hydrogen bond acid used, it is not surprising that the highly aqueous THF mobile phase has the largest negative *b* coefficient and that MeOH mobile phase, having the lowest water content, produces the smallest. However, the fact that *b* is so similar to that of the ODS phase is surprising. On the basis of LSERs describing the alkane−water partition coefficient (P_{aw}) and octanol−water partition coefficient

(41) Knox, J. H.; Kaur, B. In *High Performance Liquid Chromatography*; Brown, P., Hartwick, R., Eds.; Wiley: New York, 1989; Chapter 4.
(42) Colin, H.; Eon, C.; Guiochon, G. *J. Chromatogr.* **1976**, *122*, 223−242.
(43) Park, J. H.; Dallas, A. J.; Chau, P.; Carr, P. W. *J. Phys. Org. Chem.* **1994**, *7*, 757−769.

Table 4. Retention Correlation Across Carbon Columns[a]

phase	slope	intercept	*n*	r^b	sd[c]
		65% ACN			
Hp-C/ZrO_2	0.900 (0.02)	0.123 (0.01)	25	0.994	0.05
Cp-C/ZrO_2	0.848 (0.02)	−0.013 (0.01)	25	0.996	0.04
Io-C/ZrO_2	0.875 (0.02)	0.033 (0.01)	25	0.995	0.05
B-C/ZrO_2	0.896 (0.01)	0.104 (0.01)	25	0.997	0.04
T-C/ZrO_2	0.899 (0.02)	0.004 (0.01)	25	0.993	0.06
Od-C/ZrO_2	0.891 (0.02)	−0.218 (0.01)	25	0.993	0.06
		36% THF			
Hp-C/ZrO_2	1.046 (0.02)	−0.173 (0.02)	26	0.995	0.05
Cp-C/ZrO_2	0.852 (0.02)	0.066 (0.02)	26	0.993	0.05
Io-C/ZrO_2	0.895 (0.03)	0.105 (0.02)	26	0.984	0.08
B-C/ZrO_2	0.917 (0.02)	0.156 (0.01)	26	0.996	0.04
T-C/ZrO_2	1.004 (0.05)	−0.084 (0.04)	26	0.972	0.12
Od-C/ZrO_2	0.890 (0.04)	−0.035 (0.03)	26	0.980	0.09
		83% MeOH			
Hp-C/ZrO_2	0.907 (0.01)	0.211 (0.01)	25	0.997	0.04
Cp-C/ZrO_2	0.860 (0.01)	0.039 (0.01)	25	0.997	0.03
Io-C/ZrO_2	0.875 (0.01)	0.088 (0.01)	25	0.997	0.03
B-C/ZrO_2	0.900 (0.01)	0.127 (0.01)	25	0.998	0.02
T-C/ZrO_2	0.919 (0.05)	0.211 (0.03)	24	0.966	0.12
Od-C/ZrO_2	1.017 (0.07)	−0.131 (0.04)	25	0.946	0.17

[a] Hypercarb log k' values used as independent variable. Standard deviation in parentheses. [b] Correlation coefficient. [c] Average standard deviation of fit.

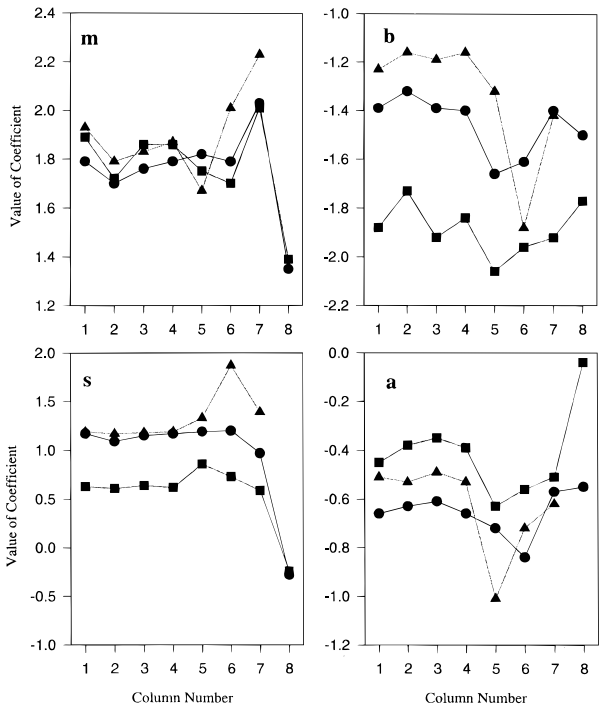

Figure 3. Plot of LSER coefficients as function of column packing and mobile phase. Conditions: same as in Figure 1. Column identification: 1, Hp-C/ZrO_2; 2, Cp-C/ZrO_2; 3, Io-C/ZrO_2; 4, B-C/ZrO_2; 5, T-C/ZrO_2; 6, Od-C/ZrO_2; 7, Hypercarb; and 8, ODS-Hypersil. Curve A, 36:64 THF/water (■). Curve B, 83:17 MeOH/water (▲). Curve C, 65/35 ACN/water (●).

(P_{ow}),[44] we had expected *b* to be rather large and negative for transfer of solutes from an aqueous/organic phase. The carbon phases examined here should not possess much, if any, ability to donate hydrogen bonds; thus, such interactions should be confined solely to the mobile phase. Consequently, solutes with hydrogen bonding acceptor ability are expected to remain in the mobile phase, and the LSER should show a very large negative coefficient. We can quantitate the degree to which *b* is smaller than expected by looking at the *b*/*m* ratios for different systems; this ratio is chosen since it is much more independent of mobile phase composition than *b* alone.[25] The *b*/*m* ratios for LSER-P_{aw} and LSER-P_{ow} are −1.10 and −0.91, respectively.[44] For acetonitrile mobile phases, *b*/*m* ratios for LSER-C18 and LSER-carbon are −1.07 and −0.80, respectively. Since we do not observe large *b* coefficients, this suggests that mobile phase is sorbed on carbon and tunes its physicochemical properties. We had expected a *b*/*m* ratio on the carbon phases more like that observed for alkane−water partitioning (−1.10).

Hydrogen Bond Acidity ($a\Sigma\alpha_2^H$). Similar to the $b\Sigma\beta_2^H$ term, this coefficient does not vary appreciably among the different carbon phases. The minor differences between phases are not surprising; however, their magnitudes are not large enough to require interpretation. The significant decrease in the magnitude of *a* upon changing to THF once again suggests strong adsorption of THF on carbon. Adsorption of the stronger hydrogen bond base mobile phase modifier (THF) on carbon makes the carbon more similar to the mobile phase; thus, we observe a small *a* coefficient.

Intercept (log k'_0). Ideally, the intercept term in the LSERs reflects only the phase ratio contribution to the capacity factor; however, based on the choice of descriptors and how well they model particular interactions, the intercept may contain additional information. If we assume that relative differences in the intercept arise from only the phase ratio contribution to retention, we can interpret the term. In an adsorption process, the phase ratio should be proportional to the surface area available for solute sorption. Since the surface areas for all the C/ZrO_2 phases are roughly the same (30 m^2 g^{-1}), we expect and observe similar values for the intercept. However, the Hypercarb packing has a considerably larger surface area (200 m^2 g^{-1}). Thus, assuming comparable chemistry, its LSER intercept should be approximately an order of magnitude larger than those on the C/ZrO_2 materials. The intercept values given in Table 3 do not exhibit this behavior; they are nearly the same for virtually all carbon phases. One possible explanation for this observation is that there is a significant energy difference between the C/ZrO_2 surface and that of Hypercarb. The C/ZrO_2 surface must have a higher adsorption energy that compensates for the surface area difference relative to Hypercarb such that the intercepts become similar. Alternatively, the presence of micropores could account for the disparity in expected intercept values; however, we can find no evidence for the existence of micropores in PGC.

Temperature Effects on Retention. On conventional bonded reversed-phase materials, an increase in column temperature typically decreases retention and often increases chromatographic efficiency.[45] In general, a 1−2 °C increase in temperature leads to a 1% change in retention.[46,47] Increasing the temperature causes an increase in the solute's solubility in the mobile phase. Additionally, it should cause an increase in the rate of desorption of a solute from the stationary phase. High temperatures also

(44) Abraham, M. H.; Chadha, H. S.; Whiting, G. S.; Mitchell, R. C. *J. Pharm. Sci.* **1994**, *83*, 1085−1100.
(45) Poole, C. F.; Poole, S. K. *Chromatography Today*; Elsevier, New York, 1991.
(46) Dolan, J. W. *LC-GC* **1990**, *8*, 842−844; **1991**, *9*, 762,764.
(47) Gilpin, R. K. *J. Chromatogr. Sci.* **1984**, *22*, 371−377.

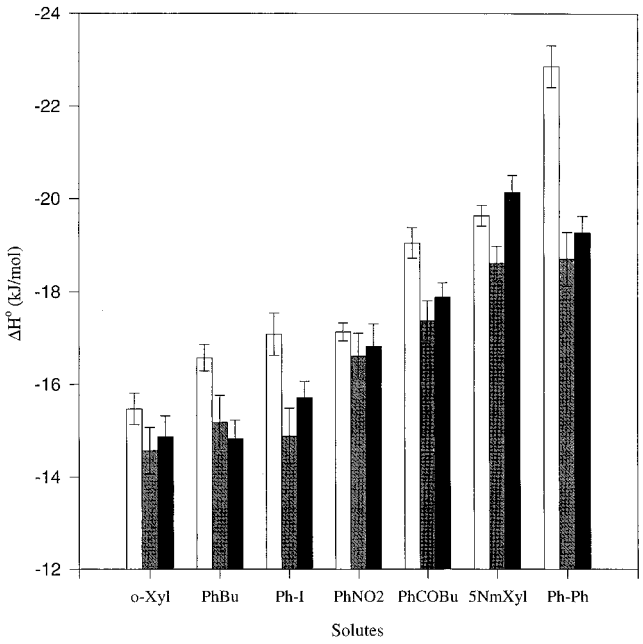

Figure 4. Dependence of ΔH on packing material and solute over temperature range 40−90 °C. Column identification: white, T-C/ZrO_2; gray, Cp-C/ZrO_2; and black, Hypercarb. Conditions: same as in Figure 1.

facilitate mass transfer of the solute in and out of the porous support.

The relationship between the logarithm of the capacity factor and the reciprocal temperature is linear for reversed-phase systems and is described by the relationship between capacity factor and free energy (shown by eqs 3 and 4). Calculation of

$$\ln k' = -\Delta G°/RT + \ln\phi \quad (3)$$

$$\ln k' = -\Delta H°/RT + \Delta S°/R + \ln\phi \quad (4)$$

the slope of the line results in a quantity directly related to the enthalpy change upon transfer of the solute from the mobile phase to the stationary phase. We utilize this relationship to further characterize the chromatographic materials studied here.

Based on previous work,[17] it appeared that the chemistry of the vapor-deposited carbon phase was related to the organic vapor used as the carbon source. For the purposes of this study, two C/ZrO_2 phases, Cp-C/ZrO_2 and T-C/ZrO_2, were chosen, and comparison measurements were conducted on Hypercarb and ODS-Hypersil. Close examination of ln k' versus reciprocal temperature plots does show some slight downward curvature, but for the present purposes they are nearly linear across the temperature range examined (r > 0.99). Figure 4 shows a comparison of the enthalpy of transfer from the mobile phase to carbon for each solute on a series of representative phases. Table 5 summarizes the data for the enthalpy and the entropy/phase ratio terms from eq 4. Generally, the carbon phases have similar enthalpies for the compounds examined, and the retention decreases are comparable to those observed with bonded phases. However, the enthalpies of retention are most similar for the Cp-C/ZrO_2 and Hypercarb materials, while the enthalpies associated with T-C/ZrO_2 are somewhat larger. The increase in adsorption enthalpy for T-C/ZrO_2 over the other materials may be due to the presence of active sites on its surface.[17] Figure 4 shows that

Table 5. Influence of Temperature on Solute Retention[a,b]

solutes	T-C/ZrO_2	Cp-C/ZrO_2	Hypercarb	ODS-Hypersil[c]
		$\Delta H°$ (kJ/mol)		
biphenyl	−22.9 (0.5)	−18.7 (0.6)	−19.3 (0.4)	−18.7 (0.5)
5-nitro-*m*-xylene	−19.6 (0.2)	−18.6 (0.4)	−20.1 (0.4)	−16.8 (0.5)
butyrophenone	−19.0 (0.3)	−17.4 (0.4)	−17.9 (0.3)	−14.0 (0.4)
nitrobenzene	−17.1 (0.2)	−16.6 (0.5)	−16.8 (0.5)	−14.6 (0.4)
butylbenzene	−16.6 (0.3)	−15.2 (0.6)	−14.8 (0.4)	−19.9 (0.7)
iodobenzene	−17.1 (0.5)	−14.9 (0.6)	−15.7 (0.4)	−17.2 (0.3)
o-xylene	−15.5 (0.3)	−14.6 (0.5)	−14.9 (0.5)	−15.0 (1.2)
		$\Delta S°/R$ + ln[phase ratio]		
biphenyl	−5.6 (0.2)	−4.4 (0.2)	−4.3 (0.1)	−4.2 (0.2)
5-nitro-*m*-xylene	−5.6 (0.1)	−5.3 (0.1)	−5.2 (0.1)	−4.3 (0.2)
butyrophenone	−6.0 (0.1)	−5.4 (0.2)	−5.3 (0.1)	−3.6 (0.2)
nitrobenzene	−5.8 (0.1)	−5.7 (0.2)	−5.7 (0.2)	−4.7 (0.1)
butylbenzene	−5.3 (0.1)	−5.0 (0.2)	−4.7 (0.2)	−3.9 (0.3)
iodobenzene	−5.6 (0.2)	−4.8 (0.2)	−5.0 (0.1)	−4.3 (0.1)
o-xylene	−5.4 (0.1)	−5.1 (0.2)	−5.0 (0.2)	−3.4 (0.4)

[a] 65:35 ACN/water, 1 mL min^{-1}, 254 nm detection, 5 μL injections. [b] Standard deviation given in parentheses. [c] 40:60 ACN/water, 1 mL min^{-1}, 254 nm detection, 5 μL injections.

the retention of biphenyl, nitroxylene, and butyrophenone on the carbon phases is most sensitive to temperature. There are some cross-overs in the retention of the seven probe solutes on Hypercarb, but not on the C/ZrO_2 materials. That is to say that the elution order changes with temperature; in particular, iodobenzene, butylbenzene, *o*-xylene, and nitrobenzene change positions. Previously we have shown that the carbon phases can be classified according to the degree of unsaturation in the carbon−carbon bonds of the source vapor.[17] It appears that the temperature effects noted here agree with this observation.

From eq 4, we see that the intercept is the sum of both an entropy and a phase ratio term. For all solutes examined on the same column packing under identical conditions, the phase ratio should be constant; the variation in the intercept term must arise from differences in the entropies of transfer. However, the large error associated with the intercept from the regression statistics makes interpretation difficult. Furthermore, we have observed no evidence for enthalpy−entropy compensation with these solutes on any phase.

Figure 5 shows the thermodynamic behavior of nitroxylene isomers on the various carbon phases. There does not appear to be any significant temperature dependence on the isomer selectivity of the phases for these compounds, and they display typical reversed-phase behavior.

CONCLUSIONS

The C/ZrO_2 and Hypercarb supports are very different from alkyl bonded phases in three ways. First, as reported by ourselves[15,16] and others,[5−7] they are much more selective for the separation of both polar and nonpolar geometrical isomers. Second, as shown here, their m values at the same mobile phase composition are greater; thus, they are more hydrophobic. Third and perhaps of the most significance, their s values are large and positive. This means that, in contrast to bonded-phase RPLC, polar non-hydrogen-bonding solutes tend to be more retained on carbon phases. That is, not only are these supports hydrophobic, but they also retain solutes through electronic ($\pi-\pi$) interactions. The LSER approach gives qualitative insight into the chemical interactions involved in the retention process but falls short due to limitations in the model. This result is very important for the

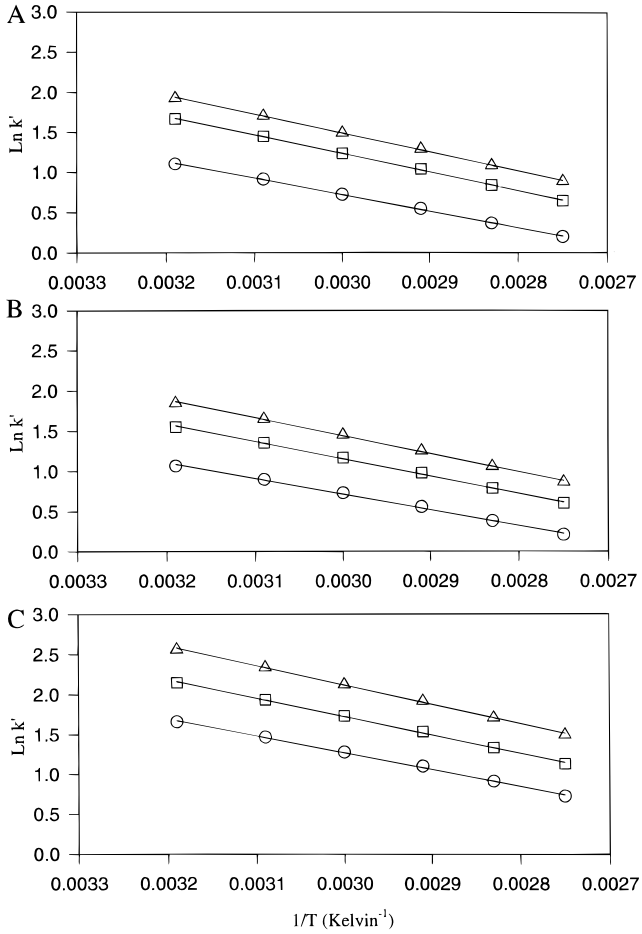

Figure 5. Temperature effects on the selectivity of nitroxylene isomers. Conditions: same as in Figure 1. (A) Cp-C/ZrO_2, (B) T-C/ZrO_2, and (C) Hypercarb. Curve 1, 2-nitro-*m*-xylene (○). Curve 2, 5-nitro-*m*-xylene (△). Curve 3, 2-nitro-*p*-xylene (□).

prediction of solute retention on carbon supports; solvophobic theory[48] is not adequate for the prediction of elution order on carbon supports due to such strong interactions with the sorbent surface.

ACKNOWLEDGMENT

This work was supported in part by grants from the Institute for Advanced Studies in Biological Process Technology at the University of Minnesota, the 3M Co., and the NIH. P.T.J. thanks the Analytical Chemistry Division of the American Chemical Society for a Summer Fellowship, sponsored by Dow Chemical Co., and Mr. Jeff Weckwerth and Mr. Mark Vitha for the many insightful discussions about LSERs.

APPENDIX

The methodology for computing the cross-sectional surface area for all of the molecules given in Table 6 is as follows. First, a structure is entered into the *Macromodel* molecular modeling system[49] via the computer mouse. The structure is then energy minimized using either the AMBER[50] molecular mechanics parameter set, as implemented in *Macromodel*, or MOPAC version 6, a semiempirical molecular orbital program.[51,52] MOPAC is used to energy minimize the structures of compounds containing the nitro groups; the AMBER force field does not contain parameters for this moiety. All MOPAC calculations are carried out using the AM1 Hamiltonian[53] and the NODIIS option.[52] The optimized structures, produced from MOPAC, are stored in the *Macromodel* format using a conversion program written in FORTRAN.

Table 6. Solute Surface Areas (Å^2)

no.	solute	$r_p = 0$	$r_p = 0.5$	$r_p = 0.61$	$r_p^{\ddagger} = 0.61$	empirical
1	benzene	35.10	48.04	51.07	36.82	51.00
2	fluorobenzene	36.97	50.36	53.47	38.89	54.40
3	chlorobenzene	39.90	53.90	57.13	42.05	56.95
4	bromobenzene	41.16	55.42	58.71	43.43	59.95
5	iodobenzene	42.92	57.55	60.91	45.38	62.05
6	toluene	40.20	54.13	57.34	42.20	57.80
7	ethylbenzene	45.18	60.14	63.58	47.69	65.45
8	propylbenzene	50.64	67.08	70.82	54.16	73.10
9	butylbenzene	55.37	73.34	77.39	60.16	80.75
10	pentylbenzene	60.70	79.92	84.28	66.53	88.40
11	acetophenone	47.70	62.94	66.43	50.11	68.00
12	propiophenone	52.78	69.23	72.98	55.98	74.80
13	butyrophenone	57.76	75.79	79.85	62.22	82.45
14	valerophenone	63.04	82.34	86.71	68.56	90.10
15	hexanophenone	68.21	88.91	93.58	74.98	97.75
16	phenol	38.01	51.60	54.73	39.94	54.40
17	benzyl alcohol	43.09	57.62	60.97	45.38	62.05
18	styrene	46.50	61.62	65.08	48.94	60.52
19	benzonitrile	41.66	56.10	59.44	44.07	56.10
20	*p*-nitrophenol	47.17	62.26	65.69	49.46	65.45
21	*p*-nitrotoluene	49.48	64.98	68.49	51.95	68.85
22	biphenyl	63.15	81.09	85.18	66.69	102.00
23	anisole	43.09	57.62	60.97	45.38	60.35
24	*N*-methylaniline	45.15	60.23	63.67	47.74	66.30
25	3-phenylpropanol	58.83	71.07	74.99	57.92	85.0
26	*o*-xylene	45.02	59.43	62.74	46.83	64.60
27	*m*-xylene	45.29	60.20	63.58	47.60	64.60
28	*p*-xylene	45.30	60.21	63.60	47.64	64.60
29	nitrobenzene	44.24	58.77	62.11	46.33	62.05

The FORTRAN program *surface_area* takes the energy-minimized structures and implements the following algorithm. The molecule structure is first repositioned in Cartesian three-dimensional space so that the center of gravity is at the origin. Next, the molecule is rotated so that most of the mass is located parallel to the *xy* plane and as near to $z = 0$ as possible. This is accomplished through the calculation of the three components of the moment of inertia and the eigenvectors for rotation to the inertial reference frame.[54]

The center of a probe disk of radius r_p is then placed initially on a vector projected from the *xy* plane origin and of angle θ and length $3L_{max} + r_p + r_{vdW}$. L_{max} is the distance between the *xy* plane origin (center of molecule mass) and the *xy* coordinates of the farthest atom, and r_{vdW} is the van der Waals radius of the farthest atom. We use the van der Waals radii compilation by Bondi;[55] these values are quite similar to the van der Waals radii used in the AMBER force field. The length of the disk is then iteratively

(48) Horvath, C.; Melander, W. R.; Molnar, I. *J. Chromatogr.* **1976**, *125*, 129−156.
(49) Mohamadi, F.; Richards, N. G. J.; Guida, W. C.; Liskamp R.; Lipton, M.; Caufield, C.; Chang, G.; Hendrickson, T.; Still, W. C. *J. Comput. Chem.* **1990**, *11*, 440−467.
(50) Weiner, S. J.; Kollman, P. A.; Case, D. A.; Singh, U. C.; Ghio, C.; Alagona, G.; Pofeta, S.; Weiner, P. *J. Am. Chem. Soc.* **1984**, *106*, 765−784.
(51) Stewart, J. J. P. *J. Comput.-Aided Mol. Design* **1990**, *4*, 1−105.
(52) MOPAC, Version 6, Available from the Quantum Chemistry Program Exchange, Indiana University, Bloomington, IN.
(53) Dewar, M. J. S.; Zoebisch, E. G.; Healy, E. F.; Stewart, J. J. P. *J. Am. Chem. Soc.* **1985**, *107*, 3902−3909.
(54) Arfken, G. *Mathematical Methods for Physicists*, 3rd ed.; Academic: New York, 1985.
(55) Bondi, A. *J. Phys. Chem.* **1964**, *68*, 441−451.
(56) Press, W. H.; Teukolsky, S. A.; Vetterling, W. T.; Flannery, B. P. *Numerical Recipes*, 2nd ed.; Cambridge University: New York, 1992.

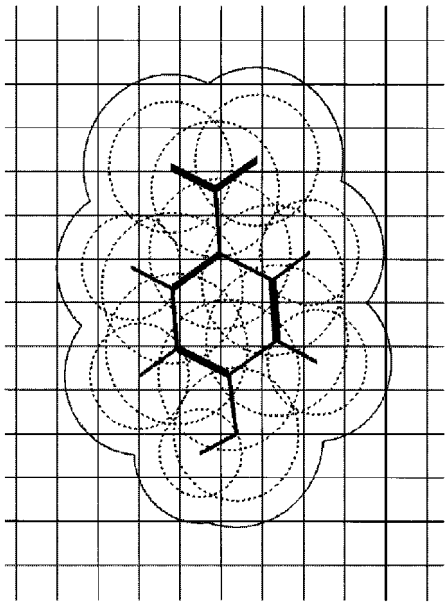

Figure 6. Outlines of the outer hull for 4-nitrophenol on a 1 Å × 1 Å grid. The solid line is the outer hull, and the dashed line is the atomic van der Waals projected radii. Thick lines represent the bonding connectivity.

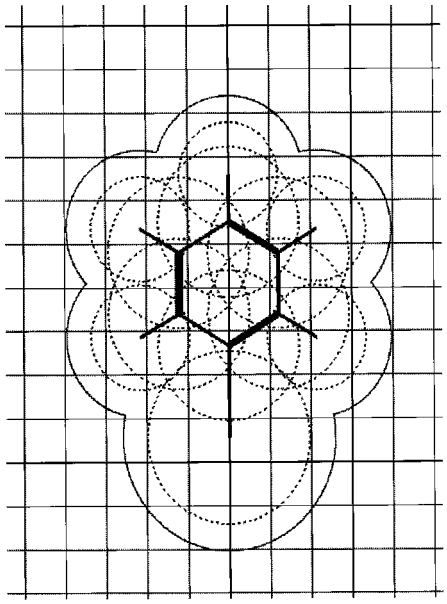

Figure 7. Outlines of the outer hull for iodobenzene on a 1 Å × 1 Å grid. The solid line is the outer hull, and the dashed line is the atomic van der Waals projected radii. Thick lines represent the bonding connectivity.

reduced using a bisection algorithm[56] until the outer edge of the disk just touches the van der Waals radius of the closest atom at θ_i. Typically, 30 iterations of bisection produces a difference in length between iterations less than 10^{-5} Å.

The *xy* location of the probe disk is then stored at angle θ_i, and the angle is incremented by a tenth of a degree and the calculation repeated. This is done until the outer hull of the molecule's projection is traced. The area traced out by the hull, as a function of angle θ_i, is then integrated by forming the triangle between the 0,0 position, the outer hull at angle θ_i (distance *a* from the origin), and the outer hull at angle θ_{i+1} (distance *b* from the origin). Integration is via the general formula for the area of a triangle: $A_i = 0.5ab \sin \theta_i$; hence, $A_{cs} = \sum_i A_i$, where A_{cs} is the cross-sectional area.

The probe radius, r_p, is chosen to be 0.61 Å for the following reason. As stated by Snyder,[31] the experimental cross-sectional surface area can be brought into agreement with calculation if 0.5 Å is added to all of the van der Waals radii. Rather than do this, which appears physically unrealistic, we can get the experimental and calculated cross-sectional area of benzene (which is noted to be 51 Å^2) into agreement by using a probe radius of 0.61 Å. We also note that, if the probe radius is 0.5 Å, there is a small difference between the surface areas which we will discuss shortly.

Another number that appears to be of interest is the cross-sectional area which is obtained when the probe radius, r_p, is finite, but the integration is performed by subtracting the r_p value from the *a* and *b* distances prior to the integration step. This quantity, which we will denote as $r_p^{\ddagger}$, is useful to see how much of the molecule is contained in the bay regions which are occluded by using a "rolling disk" approach to the area estimation.

The results of the calculations are given in Table 6 for all of the different methods of cross-sectional surface area computation described here. Also shown are Figures 6 and 7, where the outlines of the outer hulls are given for *p*-nitrophenol (Figure 6) and iodobenzene (Figure 7).

As can be seen from the numbers in Table 6 and Figures 6 and 7, the finite size of r_p makes a difference in the calculation of A_{cs}. Also shown in Table 6 is the almost constant value of approximately 3 Å^2 between the A_{cs} values for r_p of 0.5 Å and r_p of 0.61 Å.

The values shown in Table 6 are somewhat higher than those given for the adsorption of gases on solids in one of the original compilations[35] of data of this kind. However, the values in Table 6 are consistent with A_{cs} values obtained from the adsorption of solutes onto solids in the liquid phase; this is shown through the correspondence of the surface areas obtained with $r_p = 0.61$ and the column of data labeled "Empirical". The numbers which we label as empirical are from the formulas given in Snyder's book[31] which have been obtained from a large number of different solutes and categorized according to a group additivity principle. The observation that the numbers from the studies of gases adsorbed on solids[35] are smaller than those from the liquid phase is probably due to the solvent forming some type of association with the solute in the lateral direction.

The numbers in the first column of Table 6 ($r_p = 0$) are even smaller than those given in the study of gases adsorbed on solids,[35] where solvent effects are absent. This is as expected, because the space between molecules cannot be effectively packed, even without the presence of solvent. This is due to the fact that adsorbed molecules do not have a simple geometry that is conducive to nearest-neighbor packing. Furthermore, crystalline surfaces such as graphite will order the adsorbed molecules to specific orientations, which further reduces the packing effectiveness.

Finally, we note that the column of data where $r_p^{\ddagger} = 0.61$ is quite close to that for $r_p = 0$, except where long alkyl chains are present. This suggests that the selection of the proper r_p value for alkyl chains is more problematic; however, there are further questions regarding alkyl chain-adsorbed conformation which are addressed below.

A number of assumptions are present in this data and must be mentioned for completeness. First, it is reasonable to assume

that aromatic molecules lie flat on surfaces; however, it is not clear that alkyl chains will do the same, especially for short chains. Furthermore, the hydrogens may not fit in a flat adsorbed state, suggesting that some inaccuracy may be found where there are alkyl chains present. Second, the alkyl chains have all been modeled in the fully trans state; it is quite possible on real surfaces that some defects will be present in the alkyl chains, leading to smaller A_{cs} values than those computed here. Furthermore, some specific chemical effects would be visible if modeling took into account the structure of the adsorbent. For example, any hydrogen bonding between the solutes and the surface would force orientation of the solutes away from the ideal picture used here. This is also true for hydrogen bonding between the solvent and solute as far as distorting the ideal picture. The biphenyl structure is known to be staggered (i.e., not flat), and yet the AMBER force field yields a flat structure. However, when this molecule is in the adsorbed state, it probably has a flat structure because the adsorption energy is much larger than the rotational strain energy. Hence, the A_{cs} value for biphenyl is probably more realistically assessed from the flat conformation than the slightly staggered conformation. With all of these small nuances, however, the A_{cs} values given by $r_p = 0.61$ are probably within the $\pm 10\%$ accuracy level and should suffice for most chromatographic studies at that level of accuracy.

Received for review May 8, 1996. Accepted August 13, 1996.[⊗]

AC960453F

[⊗] Abstract published in *Advance ACS Abstracts,* January 1, 1997.